Diamond & Related Materials 94 (2019) 129–136

Contents lists available at ScienceDirect

Diamond & Related Materials

journal homepage: www.elsevier.com/locate/diamond

Tailoring electronic properties and Schottky barrier in sandwich heterostructure based on graphene and tungsten diselenide

P.T.T. Le[a,b], Le M. Bui[c,*], Nguyen N. Hieu[d], Huynh V. Phuc[e], B. Amin[g], Nguyen V. Hieu[f], Chuong V. Nguyen[h,*]

[a] Laboratory of Magnetism and Magnetic Materials, Advanced Institute of Materials Science, Ton Duc Thang University, Ho Chi Minh City, Viet Nam
[b] Faculty of Applied Sciences, Ton Duc Thang University, Ho Chi Minh City, Viet Nam
[c] NTT Hi-Tech Institute, Nguyen Tat Thanh University, Ho Chi Minh City, Viet Nam
[d] Institute of Research and Development, Duy Tan University, Da Nang 550000, Viet Nam
[e] Division of Theoretical Physics, Dong Thap University, Cao Lanh 870000, Viet Nam
[f] Physics Department, University of Education, The University of Da Nang, Da Nang 550000, Viet Nam
[g] Department of Physics, Hazara University, Mansehra 21300, Pakistan
[h] Department of Materials Science and Engineering, Le Quy Don Technical University, Ha Noi, Viet Nam

ARTICLE INFO

Keywords:
Graphene
vdW heterostructures
Schottky barrier
Tungsten diselenide
DFT calculations

ABSTRACT

Graphene based two-dimensional layered materials are attracting wide attention both experimentally and theoretically and show many superior properties that individual layers may not hold. In this work, we study theoretically the electronic properties of the graphene/WSe_2 van der Waals heterobilayer using the first-principle calculations. Our results demonstrate that the intrinsic electronic properties of graphene and WSe_2 monolayer are quite well preserved due to the weak van der Waals interactions. We find that the graphene/WSe_2 heterobilayer forms a *p*-type Schottky contact with the Schottky barrier height of 0.60 eV and shows a good thermoelectric material with high Seebeck coefficient at room temperature. Moreover, the *p*-type Schottky contact of the graphene/WSe_2 heterobilayer can be tailored by inserting WSe_2 monolayers to form graphene/WSe_2/WSe_2 and WSe_2/graphene/WSe_2 heterotrilayers or by applying electric field perpendicular to the heterobilayer. The *p*-type Schottky barrier decreases with the insertion of the WSe_2 layers, whereas it can be transformed to the *n*-type one when the negative electric field of -1.5 V/nm is applied. The results reveal the physical nature of the van der Waals heterostructures based on graphene and other two-dimensional transition metal dichalcogenides, which are helpful in providing a route to design graphene-based high-performance optoelectronic nanodevices, such as Schottky diodes and interlayer tunneling field-effect transistors.

1. Introduction

In the fourth industrial revolution, it is required for scientists to seek novel materials with intrinsic extraordinary and promising features, which are desirable for high-performance nanodevice applications. It is well known that the performances of nanodevices depend strongly on the physical and chemical properties of used materials. Looking beyond this field, graphene (G) and other G-like two-dimensional (2D) materials such as transition metal dichalcogenides (TMDs) [1-6], hexagonal boron nitride [7,8], monolayer metal monochalcogenides [9-12], phosphorene [13-18] and some others [19-25] have received great interests due to their superior properties, thus they are suitable for developing novel nanodevices. Among these 2D TMDs materials, the 2D WSe_2 material in single-layered and bilayered forms has recently been synthesized successfully by mechanical exfoliation [26], making it an excellent candidate to fabricate next-generation nanodevices. Unlike graphene, WSe_2 monolayer is a semiconductor. Its band gap is about 1.63 eV [27], opening at the *K* point. To date, various optoelectronic nanodevices, including field-effect transistors (FETs) [28] and light-emitting diodes (LEDs) [29] based on the WSe_2 material have been fabricated experimentally. Also, theoretical studies have been focused on controlling the electronic and photonic properties of the WSe_2 2D materials by strain, thickness and layer stacking [30-35]. These studies showed that the WSe_2 2D materials can be a potential material for next-generation nanodevices.

Currently, van der Waals (vdW) heterostructures based on

* Corresponding authors.
E-mail addresses: lethithuphuong@tdtu.edu.vn (P.T.T. Le), blminh@ntt.edu.vn (L.M. Bui), binukhn@gmail.com (B. Amin), chuongnguyen11@gmail.com (C.V. Nguyen).

https://doi.org/10.1016/j.diamond.2019.02.025
Received 2 January 2019; Received in revised form 17 February 2019; Accepted 25 February 2019
Available online 08 March 2019
0925-9635/

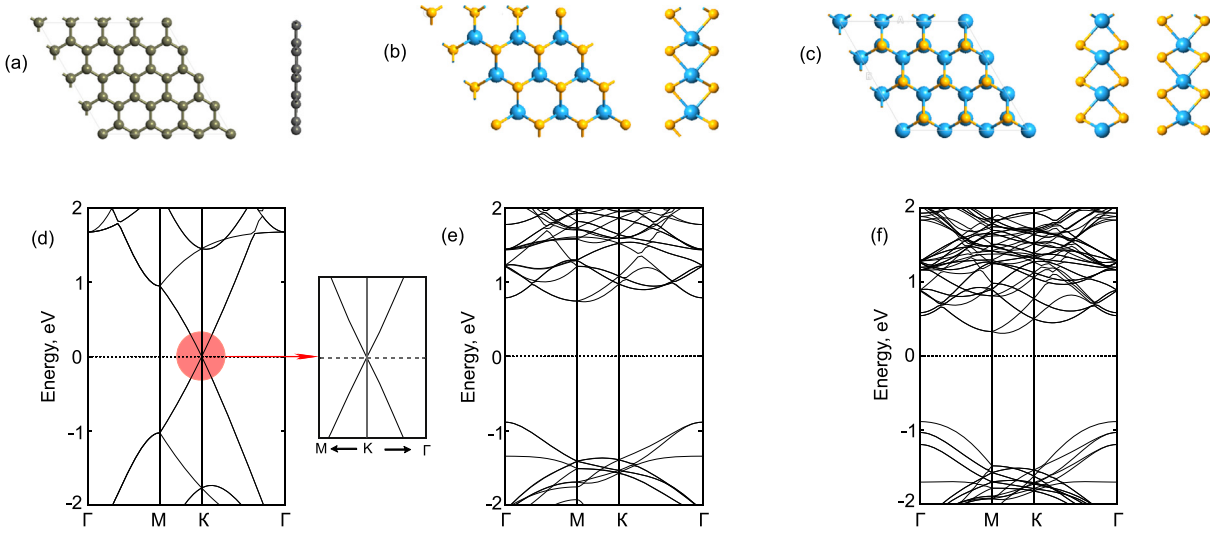

Fig. 1. (a–c) Top and side views of the atomic structures of the (4 × 4) supercell of graphene, (3 × 3) supercell of monolayer WSe_2, (3 × 3) supercell of bilayer WSe_2, respectively and (d–f) their corresponding band structures. The Fermi level is set to be zero. The inset in Fig. 1 (d) shows the linear Dirac-like dispersion around the Fermi level at the Dirac *K* point of graphene.

graphene, such as G/GaX (X = Se, S) [36-39], G/TMDs [40-42], G/phosphorene [43-45] obtained by putting the G layer on the surfaces of other semiconducting materials have also received considerable attention in both experimental and theoretical studies. These heterostructures can bring many more interesting features for novel applications in optoelectronic nanodevices which may not hold in the single layers individually. For instance, using mechanical exfoliation, a FET device with a high on/off ratio of 10^3 based on the G and GaSe monolayer has been successfully fabricated by Kim and co-workers [37]. Also, Sun and his colleagues demonstrated the preservation of the intrinsic properties in the G/phosphorene. They also suggested that this heterostructure forms an *n*-type Schottky contact and is suitable for next-generation nanodevices [43]. Recently, there have been many experimental works on the G/WSe_2 heterostructure [46,47]. Two different types of the G/WSe_2 heterostructure have been reported experimentally by Kim and his co-workers [47]. They demonstrated that such heterostructure is desirable for designing novel high-performance nanodevices, such as tunneling FETs. Also, based on the G/WSe_2 heterostructure with a Se/W vacancy defect, a barrister with a large on/off ratio at room temperature was demonstrated experimentally by Shim et al. [46]. One also investigated experimentally the band alignment of the G/WSe_2 heterostructure [47]. All these results demonstrated that the G/WSe_2 heterostructure can become a potential candidate for next-generation devices.

Therefore, in the present study, we construct an ultrathin G/WSe_2 heterobilayer and G/WSe_2/WSe_2 and WSe_2/G/WSe_2 heterotrilayers by inserting WSe_2 monolayer above G layer or below the WSe_2 part of the G/WSe_2 heterostructure. Our study focuses on the electronic properties of these sandwich heterostructures. Effects of the weak vdW interactions and external electric field on the electronic properties and the Schottky barrier of the G/WSe_2 heterostructure are also investigated in this study.

2. Computational methods

All the calculations are performed using density functional theory (DFT) and realized using Quantum Espresso code [48] with the plane-wave method. The generalized gradient approximation (GGA)–Perdew-Burke-Ernzerhof (PBE) method is utilized for describing the exchange correlation potential [49]. The complex electron-ion interactions are treated by ultrasoft pseudopotential (USPP) method for geometric optimization, energy calculations, and electronic properties. The DFT-D2 method with Grimme correction [50] is employed to describe the long-range weak vdW interactions between single-layered materials. Also, the kinetic energy of 500 eV is used for geometric optimization and energy calculations and a grid of 9 × 9 × 1 *k*-point mesh is used for the sample in the Brillouin zone (BZ). The optimization processes are considered to be converged when the atomic forces are converged to 0.001 eV/Å and the convergence threshold is set to be 10^{-6} eV. A vacuum space of 20 Å is applied to avoid any interaction between periodic images.

It should be noted that the conventional PBE method underestimates the band gap and Schottky barrier height of the heterostructures, but the Heyd-Scuseria-Ernzerhof (HSE) method may give more corrected results. Unfortunately, in this work, the hybrid function HSE and the many body GW methods are not still considered to correct these issues of the heterostructure due to the tremendously computational costs. We emphasize that our goal here is not to determine precise bandgaps and Schottky barrier heights but to illustrate the behaviors of Schottky contacts tuning by external electric fields and to uncover the underlying physics. Moreover, the PBE method is good at predicting correct trends and physical mechanisms, which possesses a guiding function for future experimental studies.

3. Results and discussion

At first, the atomic structure of the freestanding G and monolayer WSe_2 is fully relaxed to obtain the equivalent structural parameters. The lattice parameters of the freestanding G and monolayer WSe_2, respectively, are 2.47 Å and 3.32 Å. These results are in good agreement with previous experimental reports [51,52]. Thus, to construct the heterostructures based on the G and WSe_2 2D materials, we use (4 × 4) graphene cells and (3 × 3) WSe_2 cells. The lattice constant of the G/WSe_2 heterobilayer after relaxation is calculated to be 9.96 Å, implying a small lattice mismatch of only 0.8 %. In addition, we also consider the G/WSe_2 heterostructure with a 30° twist angle (by rotating the upper layer 30° about the *z* axis with the lower layer G being fixed), but the calculated binding energy is much larger than that of without rotation. It is well-known that the lower the value of the binding energy, the more stable the structure of the heterostructure. Hence, we only choose the most stable structure as an object of concrete research in our work. The atomic and electronic band structures of the (4 × 4) supercell of G, (3 × 3) supercell of WSe_2 monolayer, and (3 × 3) supercell of bilayer WSe_2 are illustrated in Fig. 1. One can observe that the pristine (4 × 4)

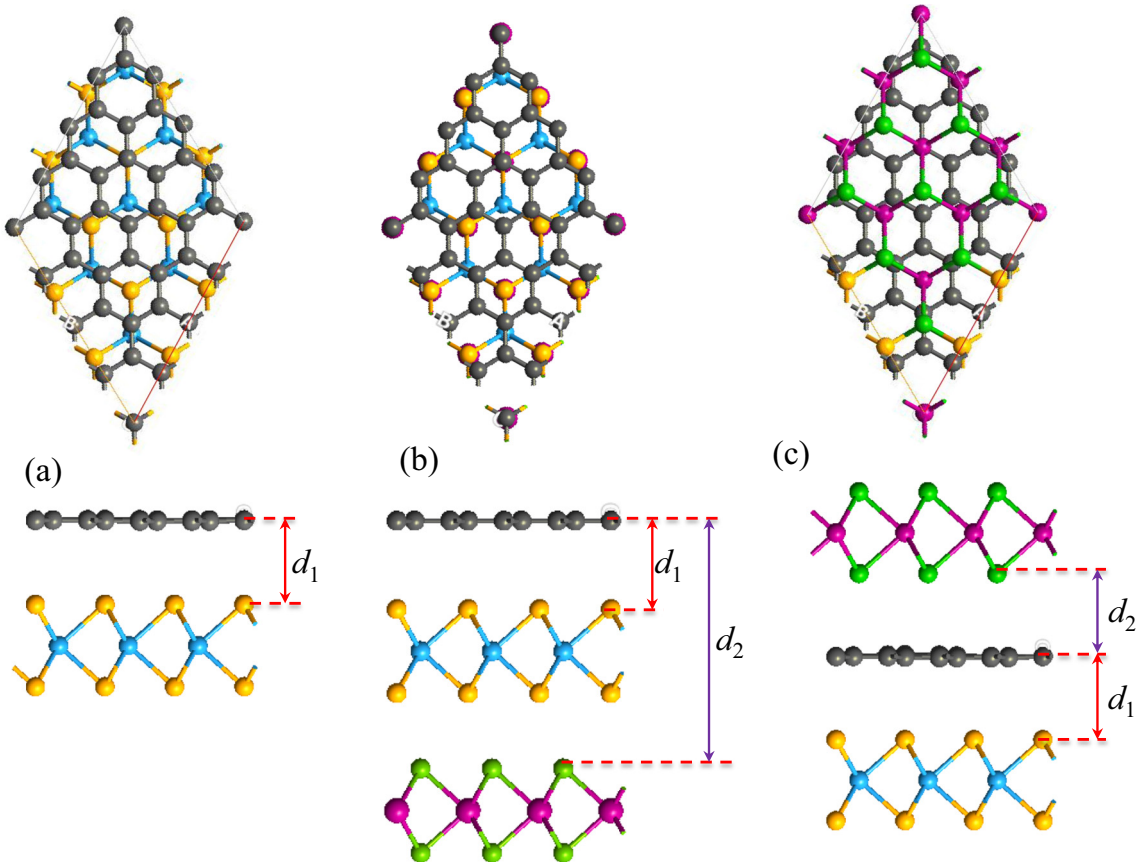

Fig. 2. Top view and side view of optimized structures of (a) G/WSe_2 heterobilayer, (b) G/WSe_2/WSe_2 and (c) WSe_2/G/WSe_2 heterotrilayers, respectively. Black balls stand for carbon atoms, yellow and blue ones stand for Se and W atoms in the first WSe_2 layer, whereas green and violet ones stand for Se and W atoms in the second WSe_2 layer.

supercell of the G is a semimetal (a zero band gap) with Dirac-like dispersion relationship around the Fermi level at the *K* point. While the (3 × 3) supercell of WSe_2 monolayer and bilayer are semiconductors with the band gap of 1.67 eV and 1.22 eV, respectively. These results are in good agreement with previous reports [53-55]. Thus, we can emphasize that the DFT-PBE method provides sufficiently reliable results. In addition, for the (1 × 1) unit cell of WSe_2 monolayer, the valence band maximum (VBM) is located at the K point [56,57]. Whereas, for the (3 × 3) supercell of WSe_2 monolayer, due to band folding effects, the VBM shifts to the Γ point as shown in Fig. 1 (b). The reason is that the inequivalent K and K' points are folded and coupled into the same Γ point when the (3 × 3) WSe_2 monolayer supercell is applied. This effect was also observed in the (3 × 3) supercell of Janus MoSeS monolayer [58].

We now construct three vdW types of heterostructures. They are (i) the G/WSe_2 heterobilayer by putting G on top of WSe_2 monolayer; (ii) the G/WSe_2/WSe_2 heterotrilayer by stacking G on top of WSe_2 bilayer; (iii) the WSe_2/G/WSe_2 heterotrilayer by sandwiching G between two WSe_2 monolayer. These structures are displayed in Fig 2. After relaxation, we can obtain the interlayer distance d_1 between the G layer and the first WSe_2 and the interlayer distance d_2 between the G layer and the second WSe_2 layer, as illustrated in Fig. 2. These values are listed in Table 1. FromTable 1, we can see that the interlayer distance between the G and WSe_2 layers in the G/WSe_2 heterobilayer is d_1 = 3.46 Å. This interlayer distance in the G/WSe_2/WSe_2 heterotrilayers [Fig. 2 (b) is d_1 = 3.52 Å. Compared with other vdW G-based heterostructures, such as G/GaSe [38,59,60], G/MoS_2 [61,62], G/phosphorene [43,63], these structures are typical vdW heterostructures where the weak vdW interactions are dominated in the considered structures. For example, Padilha et al. [63] showed that the equilibrium interlayer distance of the G/phosphorene heterostructure is 3.45 Å. Pierucci et al. [62] demonstrated that the vdW equilibrium interlayer distance of G/MoS_2 heterostructure is about 3.40 Å. Our calculations also indicate that, in the case of the WSe_2/G/WSe_2 heterotrilayer [Fig. 2 (c)], the G–top WSe_2 and G–bottom WSe_2 distances are respectively d_1 = 3.41 Å and d_2 = 3.42 Å as listed in Table 1. This also demonstrates that, in the WSe_2/G/WSe_2 heterotrilayer, all interactions between graphene and two WSe_2 layers are the weak vdW interactions. Moreover, the vertical thickness of the perfect WSe_2 monolayer is 3.350 Å, and it increases to 3.359 Å upon the formation of the G/WSe_2 heterobilayer. For the perfect WSe_2 bilayer, the vertical distance of the tungsten atoms between different layers is 6.340 Å, and it increases to 6.348 Å and to 10.201 Å upon the formation of the G/WSe_2/WSe_2 and the WSe_2/G/WSe_2 heterotrilayers, respectively.

Table 1
The interlayer distances d_1 and d_2, binding energy E_b, and *n*-type SBH $\Phi_{B,n}$ and *p*-type SBH $\Phi_{B,p}$ of the considered systems.

	d_1, Å	d_2, Å	E_b, meV/C atom	$\Phi_{B,n}$, eV	$\Phi_{B,p}$, eV
G/WSe_2	3.46	-	− 55.92	1.06	0.60
G/WSe_2/WSe_2	3.52	9.87	− 56.14	0.74	0.46
WSe_2/G/WSe_2	3.41	3.42	− 29.14	1.08	0.54

To examine the interlayer coupling and the stability in these systems, we further determine the binding energy as: $E_b = (E_{hetero} - E_G - nE_{WSe_2})/N$, where E_{hetero}, E_G, and E_{WSe_2} are the total energies of the heteromultilayers, the freestanding G, and the isolated WSe_2, respectively. *n* denotes the number of WSe_2 layers in the systems and *N* is the number of carbon atoms in the supercell. The calculated results are also listed in Table 1. As we can see, the G/WSe_2/

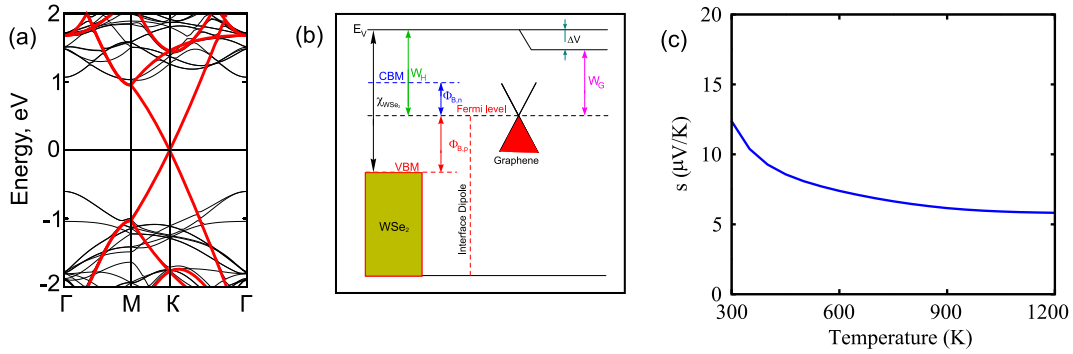

Fig. 3. (a) Projected band structure and (b) band alignment and (c) the Seebeck coefficient of the G/WSe_2 heterobilayer.

WSe_2 heterotrilayer has the lowest binding energy per carbon atom as compared with that of other heterostructures. Indeed, one can observe that all these heteromultilayers have a negative binding energy. It indicates that these systems are energetically stable and can be synthesized easily in experiment. Moreover, those binding energies have the same order of magnitude as other vdW heterostructures, such as G/phosphorene (E_b = 60 meV) [63], G/$MoSe_2$ (E_b = 53 meV) [64], G/MoS_2 (E_b = 58.1 meV) [65]. Therefore, the weak vdW interactions are dominated in these heterostructures, similar to other 2D vdW graphene-based heterostructures. Also, these considered heterostructures are feasible in experiments due to the lower binding energies.

We further consider the electronic properties of the heterobilayer obtained by putting the G layer on the WSe_2 monolayer and check how the weak vdW interactions, dominating in the G/WSe_2 heterobilayer affect its electronic properties. In Fig. 3 (a) we present the projected band structure of the G/WSe_2 heterobilayer. First, it is clear that the band structure of the G in the heterobilayer is quite well preserved with the linear Dirac-like dispersion around the Fermi level at the Dirac K point. In addition, we find that a small band gap of 8.9 meV opens in the G/WSe_2 heterobilayer around the Fermi level at the K point. Noteworthy, an opening band gap of 8.9 meV of graphene is significantly lower than k_BT (26 meV) at room temperature. It suggests that the original electronic nature of both G and WSe_2 monolayer is quite well preserved upon binding, conserving all the properties of the parent materials, a significant character for designing novel diodes based on 2D vdW heterostructures. Secondly, the WSe_2 part in the heterobilayer keeps a semiconducting behavior with a direct band gap at the Dirac Γ point. The band gap of the WSe_2 part is 1.67 eV. This value is almost unchanged as compared with that of the isolated WSe_2 monolayer. Thirdly, it can be seen that the band structure of the heterobilayer seems to be a merging between the band structures of the G layer and isolated WSe_2 layer owing to the large interlayer distances d_1 and d_2 and the negative value of the binding energies. This implies that the G/WSe_2 heterobilayer can include the greatest intrinsic properties of both G and WSe_2 layers. The similar results were also observed in other G-based heterostructures, such as G/GaSe heterostructures [59,60]. Thus, we believe that in the near future the G/WSe_2 can be used to fabricate high-performance nanoelectronic devices such as FETs. Moreover, in order to check the thermoelectric properties of such G/WSe_2 heterobilayer, we further calculate its Seebeck coefficient, as illustrated in Fig. 3 (c). The Seebeck coefficient of the G/WSe_2 heterobilayer shows that it has a good thermoelectric material with high Seebeck coefficient at room temperature. However, in order to use the G/WSe_2 heterobilayer as a component of FETs, it is very important to evaluate the strength of the Schottky barrier height (SBH), existing at the metal/semiconductor interface. Therefore, we next try to explore the contact types and the strength of the Schottky barrier at the G/WSe_2 interface, which represents a metal/semiconductor heterostructure. According to the Schottky-Mott rule [66], the n-type SBH (n-SBH) is calculated by $\Phi_{B,n} = E_C - E_F$, and the p-type SBH (p-SBH) is $\Phi_{B,p} = E_F - E_V$, where E_C, E_V and E_F are respectively the conduction band minimum, valence band maximum in the WSe_2, and the Fermi level of the G. As we can see from Table 1, the n-SBH and p-SBH of the heterobilayer, respectively, are 1.06 eV and 0.60 eV, showing that the p-type Schottky contact is formed in such heterobilayer. These Schottky barrier heights are smaller than those in other vdW heterostructures, such as G/GaSe [60], G/$MoSe_2$ [64].

Although the interactions between the G and WSe_2 layers are very weak, there may be a small band bending ΔV across the heterobilayer. The nature of the formation of the band bending is due to the difference in the work function between the G and heterobilayer. To calculate the band bending, forming across the heterobilayer, we present in Fig. 3 (b) its band alignment. We can see that the band bending across the heterobilayer is calculated by the difference in the work function of the heterobilayer (W_H) and G layer (W_G), that is $\Delta V = W_H - W_G$. Our calculated work function of the G and the heterobilayer, respectively, is 4.56 eV and 4.83 eV. It means that the band bending ΔV is 0.27 eV. From this point, we can calculate the p-SBH as $\Phi_{B,p} = I_{WSe_2} - (\Delta V + W_H)$, where I_{WSe_2} is the ionization potential of the WSe_2 semiconductor. Therefore, based on the above discussion, we find that the SBH of the heterobilayer is mainly affected by the interface dipole and the band bending, existing in the heterobilayer due to the difference in the work function of the heterobilayer and the G.

As we have mentioned above, SBH affects strongly the performance of nanoelectronic devices. Thus, we now investigate the possibilities to improve the devices performed by controlling the SBH of the heterobilayer. We first try to control the SBH by inserting WSe_2 monolayer into the heterobilayer. The inserted WSe_2 monolayer can locate below the WSe_2 part of heterobilayer, forming the G/WSe_2/WSe_2 heterotrilayer, as shown in Fig. 2 (b), or above on the G layer, forming a WSe_2/G/WSe_2 heterotrilayer, as shown in Fig. 2 (c). The projected band structures of the G/WSe_2/WSe_2 and WSe_2/G/WSe_2 heterotrilayers are illustrated in Fig. 4 (a) and Fig. 4 (b), respectively. As compared with the G/WSe_2 heterobilayer, both heterotrilayers form the p-type Schottky contact. However, we find that the p-SBH decreases from 0.60 eV in the G/WSe_2 heterobilayer to 0.54 eV in the WSe_2/G/WSe_2 heterotrilayer and to 0.46 eV in the G/WSe_2/WSe_2 heterotrilayer, respectively, as presented in Fig. 4 (c). Thus, the SBH in the G/WSe_2 heterobilayer can be controlled by inserting WSe_2 monolayer. Indeed, one can observe that in both forming heterotrilayers, the linear Dirac dispersion around the Fermi level is well kept. Thus, we believe that high carrier mobility can be obtained in these heterotrilayers and the insertion of WSe_2 monolayer is an effective way to modulate the SBH of the G/WSe_2 heterobilayer. Moreover, it can be seen that in both heterotrilayers, the intrinsic properties of the G are well preserved with the linear dispersion around the Fermi level at the Dirac K point. These results demonstrate that a high carrier mobility can be achieved in these heterotrilayers.

Furthermore, it is well known that the charge redistribution and the charge transfer in these heteromultilayers can be obtained by

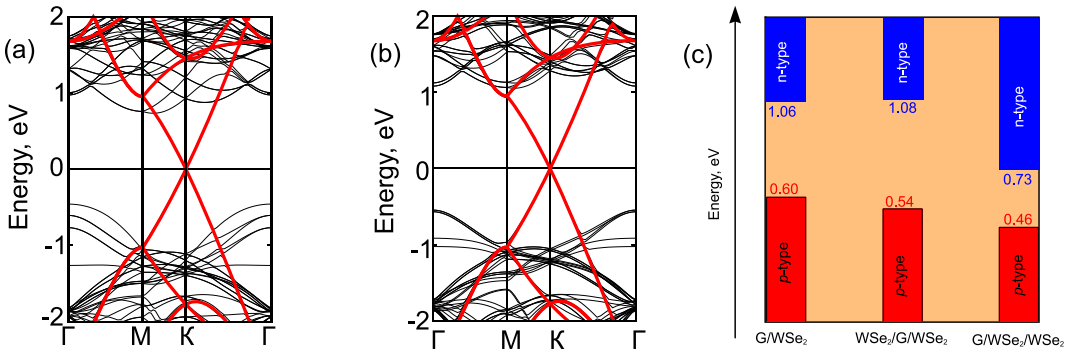

Fig. 4. Projected band structure of the G/WSe_2 heterobilayer with the insertion of the WSe_2 monolayer to form the (a) G/WSe_2/WSe_2 and (b) WSe_2/G/WSe_2 heterotrilayers. (c) The distribution of the *n*-SBH and *p*-SBH in the heterobilayer and heterotrilayers.

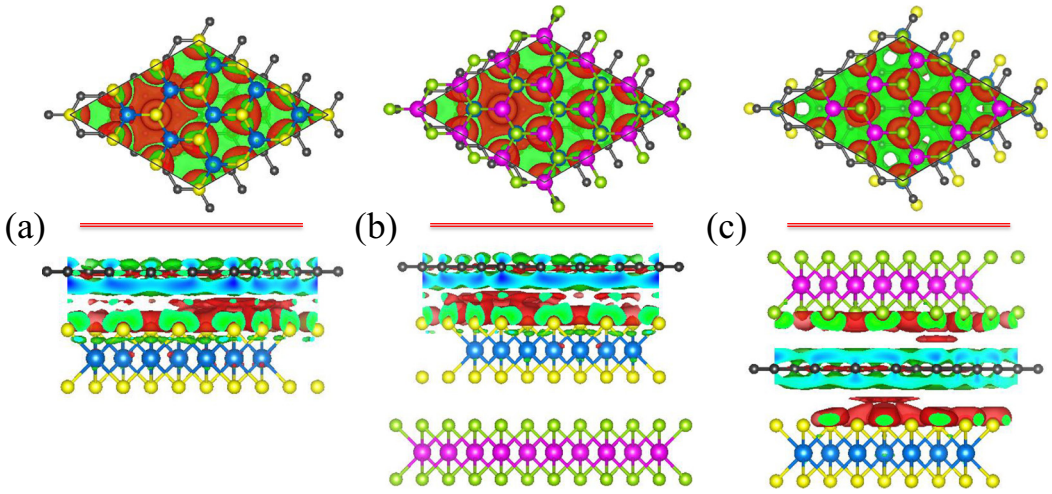

Fig. 5. Charge density difference with an isosurface of 10^{-3} *e*/Å of the (a) G/WSe_2 heterobilayer, (b) G/WSe_2/WSe_2 and (c) WSe_2/G/WSe_2 heterotrilayers, respectively. The depletion and accumulation of electrons are defined by the red and green regions, respectively.

visualizing the charge density difference, which is calculated as $\Delta\rho = \rho_H - \rho_G - n\rho_{WSe_2}$. Note that the ρ_H, ρ_G and ρ_{WSe_2} are the charge densities of the heteromultilayer, graphene, and WSe_2 monolayer, respectively. The number of the WSe_2 monolayers in the heteromultilayers is denoted by n (n = 1,2). The charge density difference in the heteromultilayers is visualized in Fig. 5 by two different areas, in which the red area represents the depletion of electrons, whereas the green area represents the accumulation of electrons. It is obvious that in the heteromultilayers, charges are depleted on the WSe_2 area and accumulated on the G area. Moreover, we find that in the G/WSe_2 heterobilayer, there is only a small amount of charge transfer of 0.072 *e* between the G layer and the WSe_2 layer. This fact implies that the inhomogeneous onsite energy of the carbon atoms in the G layer is induced by the charge transfer between the G and WSe_2 layers. On the other hand, the onsite energy of carbon atoms depends on the charge redistribution in the G layer. One can see from Fig. 5 (a) that the electron density around the two adjacent carbon atoms of the G layer is no longer equivalent in the G/WSe_2 heterobilayer. As a consequence, the charge redistribution in the G layer disrupts the degeneracy of the degeneracy of the π and π^* bands near the K point, resulting in the semiconducting character. Thus, we conclude that the inhomogeneous onsite energy of the carbon atoms is induced not by the charge transfer between the G and the WSe_2 layer but by the inhomogeneous charge distribution in the G layer caused by the WSe_2 monolayer.

Recently, it is well known that applying an external electric field (E_{ext}) is a common approach to improve the performance of nanodevices. Thus, it is interesting to consider the effect of applied E_{ext} on the electronic properties and the SBH of the G/WSe_2 heterobilayer. In order to see the how the E_{ext} affects on the electronic properties of the G/WSe_2 heterobilayer, in Fig. 6 we present the SBH variation and projected band structures of such heterobilayer under the different strength of E_{ext}. In Fig. 6 (a), we illustrate the schematic model of the E_{ext} to the heterobilayer surface. The E_{ext}, directing from the WSe_2 to the G layers is defined as the positive direction. With the presence of the E_{ext}, we find that both the *n*-SBH and *p*-SBH are also changed linearly, as shown in Fig. 6 (b). The *n*-SBH increases linearly with increasing the strength of the positive E_{ext} and decreases with increasing the strength of the negative E_{ext}. Contrary to the *n*-SBH, the *p*-SBH reduces with increasing the strength of the positive E_{ext} and raises up with increasing the strength of the negative E_{ext}. As we have mentioned above, at the equilibrium state, the G/WSe_2 heterobilayer forms the *p*-type Schottky contact. It also demonstrates that the *p*-SBH is smaller than the *n*-SBH in the heterobilayer in the absence of the E_{ext}. However, as we can see from Fig. 6 (b) the *p*-SBH is larger than the *n*-SBH in the heterobilayer when the strength of the negative E_{ext} is larger than 1.5 V/nm, as defined by the orange area. The heterobilayer, in this case, is transformed to the *n*-type Schottky contact. It demonstrates the transformation of the Schottky contact in the G/WSe_2 heterobilayer from the *p*-type to the *n*-type when the negative E_{ext} exceeds − 1.5 V/nm. The mechanism of the variation of the SBH in the heterobilayer under E_{ext} is related to the change of the band bending.

The effects of the E_{ext} on the band structures of the G/WSe_2 heterobilayer are presented in Figs. 6 (c–e). By analyzing the position of the VBM and CBM of the WSe_2 part related to the E_F of the G layer, one can observe that a negative E_{ext} makes the CBM/VBM of the WSe_2 part closer/farther to the E_F of the G, as shown in Fig. 6 (c). It means that the

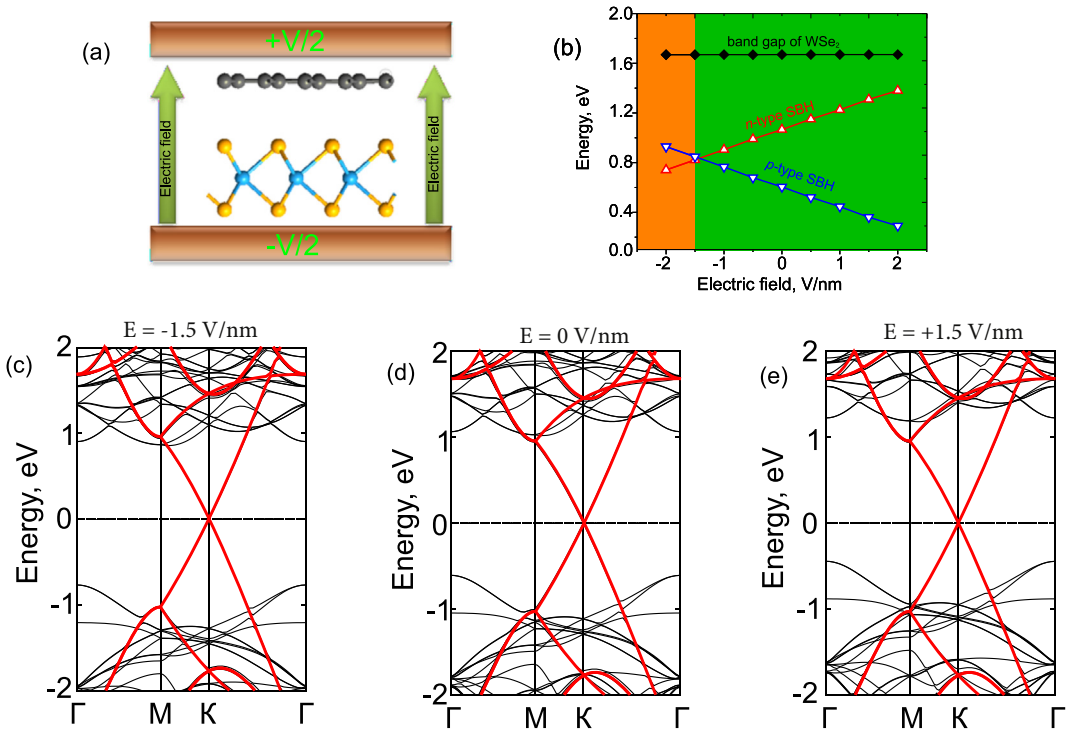

Fig. 6. (a) Schematic model of the (b) Schottky barrier of the G/WSe_2 heterobilayer (c–e) From left to right, band structures of the G/WSe_2 heterobilayer under different electric field.

p-SBH/*n*-SBH of the heterobilayer increases/decreases by applying negative E_{ext}. We can see that a negative E_{ext} smaller than − 1.5 V/nm will make a transition from the *p*-type to the *n*-type Schottky contact in the G/WSe_2 heterobilayer. This finding indicates that the G/WSe_2 heterobilayer can be used for the future Schottky electronic devices. Contrary to a negative E_{ext}, a positive E_{ext} makes the VBM/CBM of the WSe_2 part closer/farther to the E_F of the G, as illustrated in Fig. 6 (e). In the case of increasing the strength of a positive E_{ext}, the *p*-SBH decreases, whereas the *n*-SBH increases. The *p*-SBH of the heterobilayer under the positive E_{ext} of 2 V/nm decreases down to 0.29 eV from 0.60 eV at the equilibrium state. When the strength of a positive E_{ext} is larger than 2 V/nm, it can be reduced and become zero, indicating a transformation from Schottky to Ohmic contact, that is due to the linear dependence of the *p*-SBH. Our results demonstrate that not only the SBH but also the Schottky contact type can be tuned efficiently by applying the external electric field in vdW G/WSe_2 heterostructure, which may provide a promising route to design tunable Schottky diodes based on the G/WSe_2 heterostructure in the related experimental studies.

4. Conclusion

In summary, we have investigated the electronic properties of the G/WSe_2 vdW heterostructure using the first-principle calculations. We find that the G layer interacts weakly with the WSe_2 monolayer via the weak vdW interactions with a small amount of charge transfer and both the intrinsic electronic properties of the G and WSe_2 monolayers are quite well preserved in the G/WSe_2 heterobilayer. At the equilibrium interlayer distance of 3.46 Å, the G/WSe_2 heterobilayer forms the *p*-type Schottky contact with the Schottky barrier of 0.60 eV and shows a good thermoelectric material with high Seebeck coefficient at room temperature. The Schottky barrier of the G/WSe_2 heterobilayer can be tuned by inserting WSe_2 monolayer to form G/WSe_2/WSe_2, and WSe_2/G/WSe_2 heterotrilayers or by applying electric field perpendicular to the heterobilayer. The *p*-type Schottky barrier of the G/WSe_2 is 0.60 eV and it equals respectively to 0.54 eV and 0.46 eV in the case of the G/WSe_2/WSe_2 and WSe_2/G/WSe_2 heterotrilayers. When the G/WSe_2 heterobilayer is subjected to the positive electric field, a transition from the *p*-type to *n*-type Schottky contacts occurs at −1.5 V/nm, then to Ohmic contacts at −2 V/nm. These results not only provide the fundamental insights of the G/TMDs and TMDs/G/TMDs heterostructures but also a route to design high-performance optoelectronic nanodevices, such as G/WSe_2, WSe_2/G/WSe_2 Schottky diodes and interlayer tunneling FETs similar to the G/BN and G/WS_2 heterostructures [67,68].

Acknowledgments

This research is funded by Vietnam National Foundation for Science and Technology Development (NAFOSTED) under grant no. 103.01-2017.309. B. Amin acknowledges support from the Higher Education Commission of Pakistan (HEC) under Project No. 5727/261 KPK/NRPU/R&D/HEC2016.

References

[1] Q.H. Wang, K. Kalantar-Zadeh, A. Kis, J.N. Coleman, M.S. Strano, Electronics and optoelectronics of two-dimensional transition metal dichalcogenides, Nat Nanotechnol. 7 (11) (2012) 699.
[2] Q. Tang, Z. Zhou, Z. Chen, Graphene-related nanomaterials: tuning properties by functionalization, Nanoscale 5 (11) (2013) 4541–4583.
[3] D. Jariwala, V.K. Sangwan, L.J. Lauhon, T.J. Marks, M.C. Hersam, Emerging device applications for semiconducting two-dimensional transition metal dichalcogenides, ACS Nano 8 (2) (2014) 1102–1120.
[4] W.S. Yun, S. Han, S.C. Hong, I.G. Kim, J. Lee, Thickness and strain effects on electronic structures of transition metal dichalcogenides: 2H-MX_2 semiconductors (M= Mo, W; X= S, Se, Te), Phys. Rev B 85 (3) (2012) 033305.
[5] C.V. Nguyen, N.N. Hieu, N.A. Poklonski, V.V. Ilyasov, L. Dinh, T.C. Phong, L.V. Tung, H.V. Phuc, Magneto-optical transport properties of monolayer MoS_2 on polar substrates, Phys. Rev. B 96 (12) (2017) 125411.
[6] M. Yarmohammadi, The effects of strain on dc transverse and spin-valley hall conductivity of ferromagnetic moSM and silicene, J. Magn. Magn. Mater 426 (2017) 621–628.
[7] N.D. Hien, K. Mirabbaszadeh, M. Yarmohammadi, B.D. Hoi, Linear magneto-electron-light interaction in ultranarrow armchair graphene and boronitrene nanoribbons, Diamond Relat Mater. 92 (2019) 86–91.
[8] P.T. Le, M. Davoudiniya, M. Yarmohammadi, Interplay of orbital hopping and perpendicular magnetic field in anisotropic phase transitions for bernal bilayer

graphene and hexagonal boron-nitride, Phys. Chem. Chem. Phys. 21 (1) (2019) 238–245.
[9] M. Mehboudi, A.M. Dorio, W. Zhu, A. Van Der Zande, H.O. Churchill, A.A. Pacheco-Sanjuan, E.O. Harriss, P. Kumar, S. Barraza-Lopez, Two-dimensional disorder in black phosphorus and monochalcogenide monolayers, Nano Lett. 16 (3) (2016) 1704–1712.
[10] R. Fei, W. Li, J. Li, L. Yang, Giant piezoelectricity of monolayer group IV monochalcogenides: snse, sns, gese, and ges, Appl. Phys. Lett 107 (17) (2015) 173104.
[11] S. Demirci, N. Avazlı, E. Durgun, S.N. Cahangirov, Structural and electronic properties of monolayer group-III monochalcogenides, Phys. Rev. B 95 (11) (2017) 115409.
[12] C.H. Lee, S. Krishnamoorthy, D.J. O'Hara, M.R. Brenner, J.M. Johnson, J.S. Jamison, R.C. Myers, R.K. Kawakami, J. Hwang, S. Rajan, Molecular beam epitaxy of 2d-layered gallium selenide on GaN substrates, J. Appl. Phys. 121 (9) (2017) 094302.
[13] P. Le, M. Yarmohammadi, Tuning thermoelectric transport in phosphorene through a perpendicular magnetic field, Chem. Phys. 519 (2019) 1–5.
[14] H. Bui, L.T. Phuong, M. Yarmohammadi, On the influence of dilute charged impurity and perpendicular electric field on the electronic phase of phosphorene: band gap engineering, EPL (Europhysics Letters) 124 (2) (2018) 27001.
[15] D. Bui, M. Yarmohammadi, Impurity-induced anisotropic semiconductor-semimetal transition in monolayer biased black phosphorus, Phys. Lett. A 382 (28) (2018) 1885–1889.
[16] H. Bui, M. Yarmohammadi, Anisotropic electronic heat capacity and electrical conductivity of monolayer biased impurity-infected black phosphorus, Solid State Commun. 280 (2018) 39–44.
[17] P. Le, K. Mirabbaszadeh, M. Davoudiniya, M. Yarmohammadi, Charged impurity-tuning of midgap states in biased bernal bilayer black phosphorus: an anisotropic electronic phase transition, Phys. Chem. Chem. Phys. 20 (38) (2018) 25044–25051.
[18] P. Le, M. Davoudiniya, K. Mirabbaszadeh, B. Hoi, M. Yarmohammadi, Combined electric and magnetic field-induced anisotropic tunable electronic phase transition in ab-stacked bilayer phosphorene, Phys. E. 106 (2019) 250–257.
[19] B.D. Hoi, M. Yarmohammadi, Combined effect of the perpendicular magnetic field and dilute charged impurity on the electronic phase of bilayer AA-stacked hydrogenated graphene, Phys. Lett. A 382 (45) (2018) 3298–3305.
[20] M. Yarmohammadi, Perturbation tuning of plasmon modes in semiconductor armchair nanoribbons.
[21] B.D. Hoi, M. Yarmohammadi, M. Davoudiniya, Coherent control of the route of magnetic phases in quasi-1D armchair graphene nanoribbons via doping in the presence of electronic correlations, Solid State Commun. 271 (2018) 21–28.
[22] B.D. Hoi, M. Yarmohammadi, The role of electronic dopant on full band in-plane RKKY coupling in armchair graphene nanoribbons-magnetic impurity system, J. Magn. Magn. Mater. 454 (2018) 362–367.
[23] M. Yarmohammadi, Impurity doping effects on the orbital thermodynamic properties of hydrogenated graphene, graphane, in harrison model, Phys, Lett. A 380 (48) (2016) 4062–4069.
[24] S. Yarmohammadi, M. Zareyan, Bound states of dirac fermions in monolayer gapped graphene in the presence of local perturbations 25 (6) (2016) 068105.
[25] M. Yarmohammadi, Strain effects on the optical conductivity of gapped graphene in the presence of Holstein phonons beyond the dirac cone approximation, AIP Adv 6 (8) (2016) 085008.
[26] H. Li, G. Lu, Y. Wang, Z. Yin, C. Cong, Q. He, L. Wang, F. Ding, T. Yu, H. Zhang, Mechanical exfoliation and characterization of single-and few-layer nanosheets of WSe_2, TaS_2, and $TaSe_2$, Small 9 (11) (2013) 1974–1981.
[27] S.M. Eichfeld, L. Hossain, Y.C. Lin, A.F. Piasecki, B. Kupp, A.G. Birdwell, R.A. Burke, N. Lu, X. Peng, J. Li, A. Azcatl, S. McDonnell, R.M. Wallace, M.J. Kim, T.S. Mayer, J.M. Redwing, J.A. Robinson, Highly scalable, atomically thin wse_2 grown via metal-organic chemical vapor deposition, ACS Nano 9 (2) (2015) 2080–2087.
[28] H.J. Chuang, B. Chamlagain, M. Koehler, M.M. Perera, J. Yan, D. Mandrus, D. Tománek, Z. Zhou, H.J. Chuang, B. Chamlagain, M. Koehler, M.M. Perera, J. Yan, D. Mandrus, D. Tománek, Z. Zhou, Low-resistance 2d/2d ohmic contacts: a universal approach to high-performance WSe_2, MoS_2, and $MoSe_2$ transistors, Nano Lett. 16 (3) (2016) 1896–1902.
[29] J.S. Ross, P. Klement, A.M. Jones, N.J. Ghimire, J. Yan, D. Mandrus, T. Taniguchi, K. Watanabe, K. Kitamura, W. Yao, D.H. Cobden, X. Xu, Electrically tunable excitonic light-emitting diodes based on monolayer WSe_2 p-n junctions, Nat. Nanotechnol. 9 (4) (2014) 268.
[30] C.-H. Chang, X. Fan, S.-H. Lin, J.-L. Kuo, Orbital analysis of electronic structure and phonon dispersion in MoS2, MoSe2, WS2, and WSe2 monolayers under strain, 2013.
[31] B. Amin, T.P. Kaloni, U. Schwingenschlögl, Strain engineering of WS_2, WSe_2, and WTe_2, Rsc Advances 4 (65) (2014) 34561–34565.
[32] B. Amin, T.P. Kaloni, G. Schreckenbach, M.S. Freund, Materials properties of out-of-plane heterostructures of MoS_2-WSe_2 and WS_2-$MoSe_2$, Appl. Phys. Lett. 108 (2016) 063105.
[33] S. Kumar, A. Kaczmarczyk, B.D. Gerardot, Strain-induced spatial and spectral isolation of quantum emitters in mono-and bilayer WSe_2, Nano Lett. 15 (11) (2015) 7567–7573.
[34] A. Nourbakhsh, A. Zubair, M.S. Dresselhaus, T. Palacios, Transport properties of a MoS_2/WSe_2 heterojunction transistor and its potential for application, Nano Lett. 16 (2) (2016) 1359–1366.
[35] M.H. Chiu, C. Zhang, H.W. Shiu, C.P. Chuu, C.H. Chen, C.Y.S. Chang, C.H. Chen, M.Y. Chou, C.K. Shih, L.J. Li, Determination of band alignment in the single-layer MoS_2/WSe_2 heterojunction, Nat. Commun. 6 (2015) 7666.
[36] H.V. Phuc, N.H. Nguyen, B.D. Hoi, C.V. Nguyen, Interlayer coupling and electric field tunable electronic properties and Schottky barrier in graphene/bilayer-GaSe van der Waals heterostructure, Phys. Chem. Chem. Phys. 20 (2018) 17899–17908.
[37] W. Kim, C. Li, F.A. Chaves, D. Jiménez, R.D. Rodriguez, J. Susoma, M.A. Fenner, H. Lipsanen, J. Riikonen, Tunable graphene-GaSe dual heterojunction device, Adv. Mater. 28 (9) (2016) 1845–1852.
[38] Z. Ben Aziza, H. Henck, D. Pierucci, M.G. Silly, E. Lhuillier, G. Patriarche, F. Sirotti, M. Eddrief, A. ouerghi, van der Waals epitaxy of GaSe/graphene heterostructure: electronic and interfacial properties, ACS Nano 10 (10) (2016) 9679–9686.
[39] K.D. Pham, N.N. Hieu, H.V. Phuc, I. Fedorov, C. Duque, B. Amin, C.V. Nguyen, Layered graphene/GaS van der Waals heterostructure: controlling the electronic properties and Schottky barrier by vertical strain, Appl. Phys. Lett 113 (17) (2018) 171605.
[40] Y. Sata, R. Moriya, S. Morikawa, N. Yabuki, S. Masubuchi, T. Machida, Electric field modulation of Schottky barrier height in graphene/$MoSe_2$ van der Waals heterointerface, Appl. Phys. Lett 107 (2) (2015) 023109.
[41] A. Gao, E. Liu, M. Long, W. Zhou, Y. Wang, T. Xia, W. Hu, B. Wang, F. Miao, Gate-tunable rectification inversion and photovoltaic detection in graphene/WSe_2 heterostructures, Appl. Phys. Lett 108 (22) (2016) 223501.
[42] H. Coy Diaz, J. Avila, C. Chen, R. Addou, M.C. Asensio, M. Batzill, H. Coy Diaz, J. Avila, C. Chen, R. Addou, M.C. Asensio, M. Batzill, Direct observation of interlayer hybridization and dirac relativistic carriers in graphene/MoS_2 van der Waals heterostructures, Nano Lett. 15 (2) (2015) 1135–1140.
[43] M. Sun, J.P. Chou, J. Yu, W. Tang, Electronic properties of blue phosphorene/graphene and blue phosphorene/graphene-like gallium nitride heterostructures, Phys. Chem. Chem. Phys. 19 (26) (2017) 17324–17330.
[44] W. Hu, T. Wang, J. Yang, Tunable Schottky contacts in hybrid graphene-phosphorene nanocomposites, J. Mater. Chem. C 3 (18) (2015) 4756–4761.
[45] H.V. Phuc, V.V. Ilyasov, N.N. Hieu, C.V. Nguyen, Electric-field tunable electronic properties and Schottky contact of graphene/phosphorene heterostructure, Vacuum 149 (2018) 231–237.
[46] J. Shim, H.S. Kim, Y.S. Shim, D.H. Kang, H.Y. Park, J. Lee, J. Jeon, S.J. Jung, Y.J. Song, W.S. Jung, J. Lee, S. Park, J. Kim, S. Lee, Y.H. Kim, J.H. Park, Extremely large gate modulation in vertical graphene/WSe_2 heterojunction barristor based on a novel transport mechanism, Adv Mater. 28 (26) (2016) 5293–5299.
[47] K. Kim, S. Larentis, B. Fallahazad, K. Lee, J. Xue, D.C. Dillen, C.M. Corbet, E. Tutuc, Band alignment in WSe_2-graphene heterostructures, ACS Nano 9 (4) (2015) 4527–4532.
[48] P. Giannozzi, S. Baroni, N. Bonini, M. Calandra, R. Car, C. Cavazzoni, D. Ceresoli, G.L. Chiarotti, M. Cococcioni, I. Dabo, A.D. Corso, S. de Gironcoli, S. Fabris, G. Fratesi, R. Gebauer, U. Gerstmann, C. Gougoussis, A. Kokalj, M. Lazzeri, L. Martin-Samos, N. Marzari, F. Mauri, R. Mazzarello, S. Paolini, A. Pasquarello, L. Paulatto, C. Sbraccia, S. Scandolo, G. Sclauzero, A.P. Seitsonen, A. Smogunov, Quantum espresso: a modular and open-source software project for quantum simulations of materials, J. Phys.: Condens. Matter 21 (2009) 395502–395520.
[49] J.P. Perdew, K. Burke, M. Ernzerhof, Generalized gradient approximation made simple, Phys. Rev. Lett. 77 (18) (1996) 3865.
[50] S. Grimme, Semiempirical GGA-type density functional constructed with a long-range dispersion correction, J. Comput. Chem. 27 (15) (2006) 1787–1799.
[51] Y. Tang, Z. Yang, X. Dai, Trapping of metal atoms in the defects on graphene, J. Chem. Phys. 135 (22) (2011) 224704.
[52] B.W. Baugher, H.O. Churchill, Y. Yang, P. Jarillo-Herrero, Optoelectronic devices based on electrically tunable p-n diodes in a monolayer dichalcogenide, Nat. Nanotechnol. 9 (4) (2014) 262.
[53] Q. Peng, Z. Wang, B. Sa, B. Wu, Z. Sun, Electronic structures and enhanced optical properties of blue phosphorene/transition metal dichalcogenides van der Waals heterostructures, Sci. Rep. 6 (2016) 31994.
[54] H. Henck, Z. Ben Aziza, D. Pierucci, F. Laourine, F. Reale, P. Palczynski, J. Chaste, M.G. Silly, F. m. c. Bertran, P. Le Fèvre, E. Lhuillier, T. Wakamura, C. Mattevi, J.E. Rault, M. Calandra, A. Ouerghi, Electronic band structure of two-dimensional ws_2/graphene van der Waals heterostructures, Phys. Rev. B 97 (2018) 155421.
[55] N.R. Wilson, P.V. Nguyen, K. Seyler, P. Rivera, A.J. Marsden, Z.P.L. Laker, G.C. Constantinescu, V. Kandyba, A. Barinov, N.D.M. Hine, X. Xu, D.H. Cobden, Determination of band offsets, hybridization, and exciton binding in 2D semiconductor heterostructures, Sci. Adv. 3 (2) (2017) e1601832.
[56] A. Kumar, P. Ahluwalia, A. Kumar, P. Ahluwalia, Electronic structure of transition metal dichalcogenides monolayers 1H-MX_2 (M = Mo, W; X = S, Se, Te) from ab-initio theory: new direct band gap semiconductors, Eur. Phys. J. B 85 (6) (2012) 186.
[57] D. Muoi, N.N. Hieu, H.T. Phung, H.V. Phuc, B. Amin, B.D. Hoi, N.V. Hieu, L.C. Nhan, C.V. Nguyen, P.T.T. Le, Electronic properties of WS2 and WSe2 monolayers with biaxial strain: a first-principles study, Chem. Phys. 519 (2019) 69–73.
[58] Y. Li, J. Wang, B. Zhou, F. Wang, Y. Miao, J. Wei, B. Zhang, K. Zhang, Tunable interlayer coupling and Schottky barrier in graphene and janus mosse heterostructures by applying an external field, Phys. Chem. Chem. Phys. 20 (37) (2018) 24109–24116.
[59] Z. Ben Aziza, V. Zólyomi, H. Henck, D. Pierucci, M.G. Silly, J. Avila, S.J. Magorrian, J. Chaste, C. Chen, M. Yoon, K. Xiao, F. Sirotti, M.C. Asensio, E. Lhuillier, M. Eddrief, V.I. Fal'ko, A. Ouerghi, Valence band inversion and spin-orbit effects in the electronic structure of monolayer GaSe, Phys. Rev. B 98 (11) (2018) 115405.
[60] C. Si, Z. Lin, J. Zhou, Z. Sun, Controllable Schottky barrier in GaSe/graphene heterostructure: the role of interface dipole, 2D Mater 4 (1) (2016) 015027.
[61] D. Pierucci, H. Henck, C.H. Naylor, H. Sediri, E. Lhuillier, A. Balan, J.E. Rault, Y.J. Dappe, F. Bertran, P.L. Fèvre, A.T.C. Johnson, A. Ouerghi, Large area molybdenum disulphide-epitaxial graphene vertical van der Waals heterostructures, Sci Rep. 6 (2016) 26656.
[62] D. Pierucci, H. Henck, J. Avila, A. Balan, C.H. Naylor, G. Patriarche, Y.J. Dappe, M.G. Silly, F. Sirotti, A.T.C. Johnson, M.C. Asensio, A. Ouerghi, Band alignment and

minigaps in monolayer MoS_2-graphene van der waals heterostructures, Nano Lett. 16 (7) (2016) 4054–4061.
[63] J. Padilha, A. Fazzio, A.J. da Silva, Van der waals heterostructure of phosphorene and graphene: tuning the Schottky barrier and doping by electrostatic gating, Phys. Rev. Lett 114 (6) (2015) 066803.
[64] F. Zhang, W. Li, Y. Ma, X. Dai, F. Zhang, W. Li, Y. Ma, X. Dai, Strain effects on the Schottky contacts of graphene and $MoSe_2$ heterobilayers, Phys. E. 103 (2018) 284–288.
[65] W. Hu, T. Wang, R. Zhang, J. Yang, Effects of interlayer coupling and electric fields on the electronic structures of graphene and mos 2 heterobilayers, J. Mater. Chem. C 4 (9) (2016) 1776–1781.
[66] J. Bardeen, Surface states and rectification at a metal semi-conductor contact, Phys Rev 71 (10) (1947) 717.
[67] L. Britnell, R.V. Gorbachev, R. Jalil, B.D. Belle, F. Schedin, A. Mishchenko, T. Georgiou, M.I. Katsnelson, L. Eaves, S.V. Morozov, N.M.R. Peres, J. Leist, A.K. Geim, K.S. Novoselov, L.A. Ponomarenko, Field-effect tunneling transistor based on vertical graphene heterostructures, Science 335 (6071) (2012) 947–950.
[68] T. Georgiou, R. Jalil, B.D. Belle, L. Britnell, R.V. Gorbachev, S.V. Morozov, Y.J. Kim, A. Gholinia, S.J. Haigh, O. Makarovsky, L. Eaves, L.A. Ponomarenko, A.K. Geim, K.S. Novoselov, A. Mishchenko, Vertical field-effect transistor based on graphene-WS_2 heterostructures for flexible and transparent electronics, Nat. Nanotechnol 8 (2) (2013) 100.